Statistical Channel Impulse Response Models for Factory and Open Plan Building Radio Communication System Design

Theodore S. Rappaport, *Member, IEEE,* Scott Y. Seidel, *Student Member, IEEE,* and Koichiro Takamizawa, *Student Member, IEEE*

***Abstract*—This paper presents statistical radio channel impulse response models for the analysis and design of wireless factory and open plan office communication systems. The models incorporate first- and second-order statistics to characterize the discrete impulse responses of indoor radio channels for both line-of-sight (LOS) and obstructed (OBS) topographies. The effects of large scale transmitter–receiver (T–R) separation distance, small scale receiver movement, and models for the correlation of multipath component amplitudes over one meter local areas are developed from 1.3 GHz measurements reported in [1]. SIRCIM, a computer simulator based upon the models presented in this paper, has recreated multipath power delay profiles and CW fading profiles that are highly representative of measured data. Large scale models for path loss are implicitly included in this work.**

I. Introduction

DUE to previous lack of interest by the manufacturing sector, wide-band in-building propagation models for factories and open plan buildings have not been researched. Recently, however, there has been interest by the Digital European Cordless Telephone 802.4L and the IEEE 802.11 standards committees to develop indoor radio systems which accommodate data rates in excess of 1 Mb/s. Flexible wireless communications will be used for voice and data networks that link portable computers, vision systems, cash registers, and telephones in offices and factories of the future. Radio will also be required for communications to large fleets of autonomous guided vehicles (AGV's) likely to be used in manufacturing [6]. To support the anticipated capacity required within buildings, wide bandwidths and efficient multiple access techniques will be needed. Determination of suitable wireless in-building system designs requires knowledge of the different propagation environments likely to be encountered.

To date, there have been several works pertaining to the measurement and modeling of indoor radio communications in partitioned office buildings (for example, [2]–[5], [7]–[9]).

Paper approved by the Editor for Radio Communications of the IEEE Communications Society. Manuscript received November 5, 1989; revised June 24, 1990. This work was supported in part by a grant from the Purdue University Computer Integrated Design, Manufacturing, and Automation Center (CIDMAC), and by a National Science Foundation Graduate Research Fellowship.

The authors are with the Bradley Department of Electrical Engineering, Mobile and Portable Radio Research Group, Virginia Polytechnic Institute and State University, Blacksburg, VA 24061.

IEEE Log Number 9144550.

A model for indoor radio propagation in office buildings was developed in [2], and was subsequently used to perform bit error rate studies in [3]. In [4], empirical measurements and a simple two-ray Raleigh fading model were used to simulate communication system performance inside office buildings. Work in [7] and [8] has measured delay spread and path loss characteristics within several buildings. Measurements in [1], however, were made in five open plan factory buildings and revealed that such buildings typically have median rms delays spread values which are several times larger than reported in [2]. More recent measurements in factory buildings [9] have confirmed that delay spreads can be several times greater in unpartitioned factory buildings as compared to partitioned office buildings. Some statistical modeling of indoor factory channels has been reported in [10] using the measured data reported in [1], but those models do not incorporate the effects of path loss as a function of transmitter–receiver (T–R) separation. Thus, it is not possible to use [10] in system design applications where power levels must be known.

This paper presents statistical impulse response models that have been derived from measurements reported in [1]. There are compelling reasons why a *statistical* channel model is useful for indoor environments. First, the number of potential reflectors is too large to incorporate into a purely deterministic propagation model. In addition, the locations of potential scatterers vary considerably as transmitters and receivers are moved within a building, and from building to building. While it should be possible to incorporate a limited number of specular reflectors by ray tracing and diffraction theory, careful measurements which yield scattering parameters for walls, ceilings, and other common objects in buildings have not yet been reported in the literature.

Factory and open plan building radio channels may be divided into two general categories: line-of-sight and obstructed topography. When there is a direct optical path between the transmitter and receiver, line-of-sight (LOS) topography exists; absence of such a path indicates an obstructed (OBS) topography. The models presented here describe: the distribution of the number of multipath components in a particular multipath delay profile; the distribution of the number of multipath components received within a local area; the probability of receiving each multipath component at a particular excess delay; the distributions of the amplitudes, phases, and time delays of multipath components received within a local area;

0090–6778/91/0600–0794$01.00

and the probability of receiving a multipath component at small scale locations. Correlation between multipath component amplitudes at constant excess delays and small receiver separations, and at small time delay differences for the same receiver location, are also modeled from the empirical data in [1].

In addition to the development of the statistical models, we have incorporated the models into a propagation simulation program. SIRCIM creates multipath channel power delay profiles with the same ensemble and local statistics as the measured data. With this simulation tool, we can predict arriving signals at a receiver from one (or many) transmitters by performing convolutions of transmitted signals with simulated channels. These statistical channel models will be useful in assessing viable multiple access, coding, and diversity techniques, cochannel interference detection algorithms, and suitable physical layouts for high data rate factory and open plan office building radio communication systems.

II. Impulse Response Channel Model

A. Overview

The impulse response $h(t)$ of a linear systam is a useful characterization of the system since the output of the system can be computed through convolution of the applied input with the impulse response. We model multipath channels as a linear filter with a complex baseband impulse response. This has been shown to be a good model for other radio channels such as the ionosphere or troposphere [11], urban mobile radio [12]–[15], and indoor radio channels [1], [2], [7], [10].

The discrete low-pass complex channel impulse response $h_b(t)$ is given by

$$h_b(t) = \sum_k \alpha_k e^{-j\theta_k}\, \delta(t - \tau_k). \tag{1}$$

In (1), α_k represents a real voltage attenuation factor, $e^{-j\theta_k}$ represents a linear phase shift due to propagation and additional phase shifts induced by reflection coefficients of scatterers, and τ_k is the time delay of the kth path in the channel with respect to the arrival time of the first arriving component.

By using a transmitter that gates an RF carrier with a square pulse $p(t)$, the baseband output of a wideband receiver closely approximates the impulse response $h_b(t)$ of the radio channel [1], [2]. Square law envelope detection yields an estimate of the power impulse response given by

$$|h_b(t)|^2 = \sum_k \alpha_k^2 p^2(t - \tau_k). \tag{2}$$

Equation (2) assumes there is at most one multipath component and no pulse overlap within a time window equal to the duration of probe $p(t)$. The measured data from which our models are based were collected from 50 different measurement locations within five different factory buildings, although data from 6 measurement locations were inadvertently lost during transport from Purdue University to Virginia Tech where the models were developed. Details on measurement procedure are given in [1].

The power impulse responses were quantized into bins each having temporal widths of 7.8 ns (the temporal resolution of the probe). Within each bin, the discrete oscilloscope α_k^2 values were averaged using a linear spline technique to obtain an equivalent A_K^2 at a discrete excess time delay T_K. Thus, the estimate of the power impulse response (2) is modeled by

$$|h_b(t)|^2 = \sum_K A_K^2\, \delta(t - T_K) \tag{2a}$$

where A_K^2 is a measure of multipath power and A_K is the real voltage envelope in the time window equal to the duration of probe. Note a particular A_K may include the effects of several arriving components within a bin as the individual components add vectorially at the receiver antenna. This will result in signal fading within the bin over small spatial locations. An example of the linear spline averaging technique used to determine A_K^2 is shown in Fig. 1(a) where the α_k^2 values contained within an excess delay interval are given equal weighting, and adjacent α_k^2 values are weighted one half of those within the interval. A maximum of 64 resolvable discrete multipath components are separated by integral multiples of 7.8 ns since the oscilloscope time domain window size was not greater than 500 ns for 49 of the 50 original measurement sites. Therefore, the models are based upon the assumption that no multipath components arrive at excess delays greater than 500 ns, although multipath components occasionally arrive at excess delays greater than 500 ns. A minimum received power threshold of 48 dB below a 2.3 m free space reference was used to threshold the individual multipath components, based on the maximum dynamic range of the receiver (~90 dB). The threshold corresponds to a minimum SNR threshold of 6 dB for a detectable multipath pulse, although most components arrive with SNR greater than 10 dB. Fig. 1(b) shows a received power profile, the corresponding data reduction, and the noise threshold line; all components below the line are considered to be noise, and are not used in computation of channel statistics. Examples of actual multipath power delay profiles measured in a LOS topography and an OBS topography are given in Figs. 2 and 3.

Because power delay profile impulse responses were recorded at $\lambda/4$ intervals on a 1 m track at each measurement location, we are able to characterize local, small scale, fading of individual multipath components and the small scale variation in the number and arrival times of multipath components. Thus, the statistical models are functions of time delay, small scale receiver spacing within a 1 m local area, topography, large scale $T-R$ separation, and the particular measurement location. Let P represent the set of all measured 1 m local areas and let X denote the set of small scale locations equally spaced along a 1 m track in a particular local area. Then, a particular measurement location can be denoted by $P_n \in P$ where n ranges on 1 to 44, and a particular small scale location of a profile measured in location P_n can be denoted by X_l where $X_l \in X$ and l ranges on 1 to 19. Furthermore, each local area measurement was made in a location classified by a particular topography $S_m \in S = \{S_1, S_2\}$ where S_1 denotes a LOS topography, and S_2 denotes an OBS tkpography, and each location P_n has associated with it some large scale $T-R$ separation $D_n \in D$

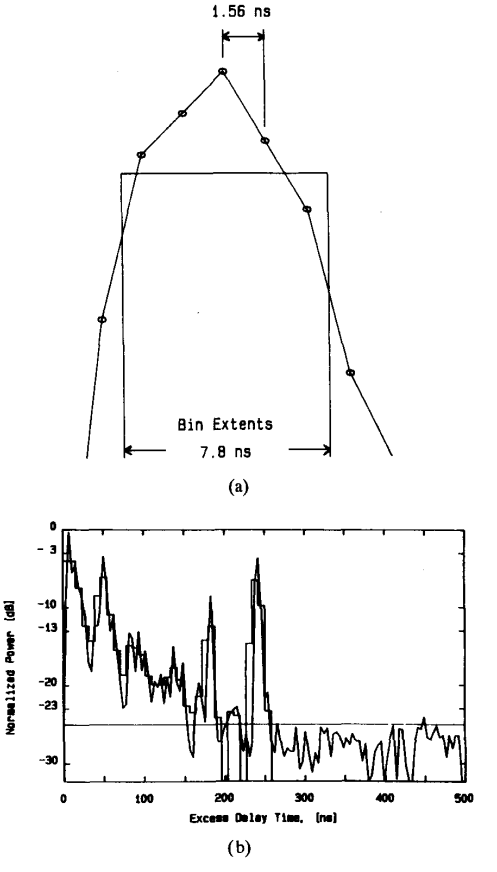

Fig. 1. Example of linear spline technique used to convert displayed oscilloscope waveform into bins. (a) Spline technique. (b) Actual profile converted into bins.

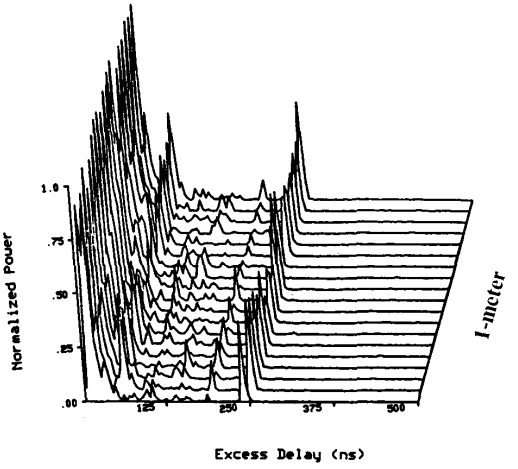

Fig. 2. Example of measured LOS profiles at 19 discrete receiver locations along a 1 m track. $T-R$ separation is 18 m.

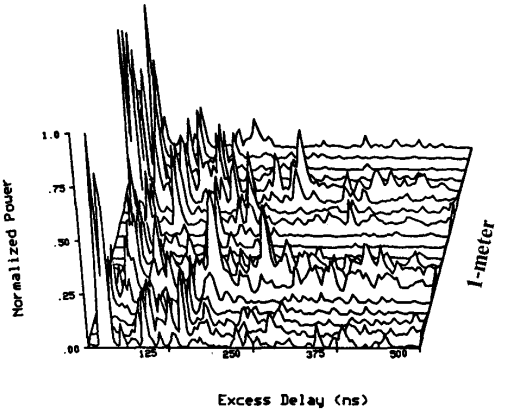

Fig. 3. Example of measured OBS profiles at 19 discrete receiver locations along a 1 m track. $T-R$ separation is 20 m.

where D is the set of $T-R$ separations corresponding to the measurement location set P. The D_n from measurements in [1] are approximately uniformly distributed between 15 m and 65 m for LOS topography locations and between 15 m and 50 m for OBS topography locations, although multipath signal levels greater than 6 dB above the receiver noise floor were detected for values of D_n as large as 80 m in [1]. Each individual baseband power delay profile can be expressed as

$$|h_b(t, X_l, S_m, D_n, P_n)|^2 = \sum_K A_K^2(T_K, X_l, S_m, D_n, P_n)\,\delta(t - T_K(X_l, S_m, D_n, P_n)). \tag{3}$$

It is reasonable to assume X, S, and D affect the impulse response independently although S and D are conditioned on the particular measurement location P. In this paper, dependence on the measurement location shall be implicitly assumed and we will omit P in many subsequent formulations except when necessary to indicate a particular measurement location P_n. Fluctuations of discrete multipath amplitudes A_K, and excess delays T_K, are statisticalhy modeled over the set P as functions of X, S, and D.

B. Multipath Channel Parameters

Wide-band multipath channels can be grossly quantified by their mean excess delay ($\overline{\tau}$) and rms delay spread (σ) [1], [2], [4]–[9], [16]–[18]. The mean excess delay is the first moment of the power delay profile and is defined to be

$$\overline{\tau} = \frac{\sum_k \alpha_k^2 \tau_k}{\sum_k \alpha_k^2} \simeq \frac{\sum_K A_K^2 T_K}{\sum_K A_K^2}. \tag{4}$$

The rms delay spread is the square root of the second central moment of the power delay profile and is defined to be

$$\sigma = \sqrt{\overline{\tau^2} - (\overline{\tau})^2} \quad \text{where } \overline{\tau^2} = \frac{\sum_k \alpha_k^2 \tau_k^2}{\sum_k \alpha_k^2} \simeq \frac{\sum_K A_K^2 T_K^2}{\sum_K A_K^2} \tag{5}$$

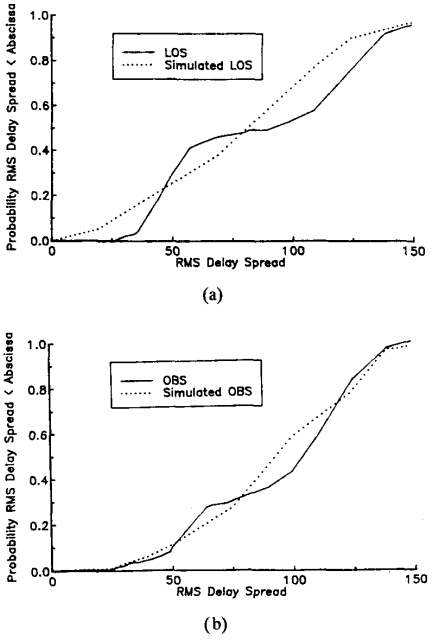

Fig. 4. Cumulative distribution function of rms delay spread of measured (a) LOS and (b) OBS factory radio channels from [1]. Also shown are results of computer simulations for the same number of measurement locations using the models presented in this paper.

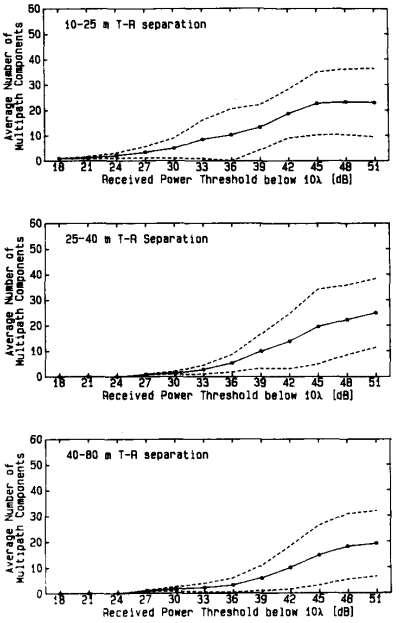

Fig. 5. Average and standard deviation of the number of detected multipath components N_p with respect to received power threshold for different $T-R$ separations.

where α_k^2 and τ_k are derived directly from the digitized oscilloscope values at the receiver, but A_K^2 and T_K values are used in modeling. In (4) and (5), the delays of each profile are measured relative to a first detectable signal arriving at $T_0 = 0$. The A_K^2 are implicitly functions of T_K, X, S, D, and P as in (3), and the term $\sum_K A_K^2$ in (4) and (5) is a relative measure of received power for a given profile. The cumulative distribution functions (cdf's) of the rms delay spread of measured LOS and OBS factory radio channels are given in Fig. 4(a) and (b) where σ was computed for each individual power delay profile at each measurement location. Also shown in the figures are the cdf's of rms delay spread for the identical number of simulated measurement locations based on the models discussed subsequently in this paper. Rms delay spread was shown in [1] to be primarily a weak function of S. The median value of rms delay spread is slightly greater in obstructed topographies (105 ns) than in line-of-sight topographies (95 ns) [1].

C. Distribution of the Number of Multipath Components

Knowledge of the number of multipath components is important for evaluating the performance of various types of diversity, modulation, and equalization techniques (i.e., RAKE receiver [19, pp. 471, 486–489]). The number of resolvable multipath components also impacts the choice of the form of the channel model. If there are a small number of paths (less than 5, which can be attributed to obvious reflecting objects in the channel), then a ray-tracing model based on geometry would seem plausible. However, when many multipath components arrive at the receiver, geometrical models are computationally difficult and are site specific. In this case, a statistical model is a useful tool for analysis. For these models, a multipath component measured in a particular profile is defined to arrive at the receiver at a particular excess delay T_K if the integrated power within a discrete excess delay interval A_K^2 [see Fig. 1(a)] is greater than the minimum detectable signal threshold of the receiver. A_K is set to zero and a multipath component does not exist if A_K^2 does not exceed the minimum detectable signal threshold at excess delay T_K.

The number of multipath components, denoted by N_p, has been computed for each of the 836 measured profiles [21]. Fig. 5 shows the average and standard deviation of the number of detected multipath components with respect to received power threshold for three different $T-R$ separation intervals. The solid line indicates the average number of multipath components and the dotted lines represent the standard deviations about the mean. At the lowest threshold levels (45 dB to 51 dB below the reference power level measured at 2.3 m), the average number of multipath components is very similar for all ranges of $T-R$ separation. It can be seen that as $T-R$ separation increases, fixed N_p occurs at successively weaker power levels due to radio path loss. Fig. 5 indicates it is reasonable to model N_p independent of $T-R$ separation at maximum receiver sensitivity. A good test for an accurate impulse response model is to apply a higher power threshold to a series of simulated impulse responses to see that they conform to Fig. 5. We have done this in [20].

The distribution of N_p over each local area (i.e., the

distribution of $N_p(X, S_m, P_n)$) is nearly always Gaussian distributed with a mean of $\overline{N}_p(S_m, P_n)$ and a standard deviation $\sigma_p(S_m, P_n)$ [20]. A typical example is shown in Fig. 6 where the empirical distribution of $N_p(X, S_1, P_6)$ is compared to a Gaussian distribution with an $\overline{N}_p(S_1, P_6)$ of 14.5 and $\sigma_p(S_1, P_6)$ of 3.6 multipath components. Since only 19 points are used to compile the local distributions, we cannot determine true distributions with great confidence. However, nearly all of the cdf's exhibit symmetry about the mean and typically fit as well as in Fig. 6. $\overline{N}_p(S_m, P_n)$ itself is a random variable which has been modeled based on the distribution of the average number of multipath components at each P_n. $\overline{N}_p(S_1, P_n)$ is uniform from 9 to 35 multipath components. For OBS topographies, $\overline{N}_p(S_2, P_n)$ is uniformly distributed from 11 to 36 multipath components. The standard deviation $\sigma_p(S_m, P_n)$ of the Gaussian distribution about $\overline{N}_p(S_m, P_n)$ is linearly related to $\overline{N}_p(S_m, P_n)$. For LOS, a linear regression on the empirical data based upon minimum mean squared error criterion yields

$$\sigma_p(S_1, P_n) = 0.492 \times \left(\overline{N}_p(S_1, P_n) - 4.77\right). \quad (6)$$

In obstructed topographies, the linear regression is

$$\sigma_p(S_2, P_n) = 0.383 \times \left(\overline{N}_p(S_2, P_n) - 0.89\right). \quad (7)$$

Fig. 7 shows the models for the relationship between $\overline{N}_p(S_m, P_n)$ and $\sigma_p(S_m, P_n)$ at each P_n superimposed on a scatter plot of the empirical data for a) LOS and b) OBS topographies. Each data point represents the statistics of the measured number of components within each local area. The straight lines in Fig. 7(a) and (b) are (6) and (7), respectively. The data indicate that the statistics of the number of received multipath components is comparable in LOS and OBS topographies. This result is not surprising when one considers that most multipath components are due to reflections from surrounding objects which will have approximately equal likelihood of being received in LOS and OBS topographies in spacious, open plan areas

D. Probability of Multipath Component Arrival

Once the number of multipath components N_p is found for a particular profile X_l, it is necessary to know the arrival time of each multipath component. The probability that a multipath component will arrive at a receiver at a particular excess delay, denoted by $P_R(T_K, S_m)$, is assumed to be independent of large scale distance D_n. This was shown to be valid in [21], and is reasonable since the large scale distance D_n corresponds to the $T-R$ separation (minimum propagation delay) and not the excess path length (excess delay) a transmitted pulse would traverse. In [1], it was shown that $T-R$ separation in open plan factories does not effect rms delay spreads or profile shapes; however, this does not appear to be valid for partitioned office buildings [7]. Fig. 8 shows $P_R(T_K, S_m)$, the empirical probability that a multipath component will be detected with an amplitude greater than the minimum threshold level, for a) LOS and b) OBS topographies. The probability has been computed by counting the total number of detected multipath components at a particular discrete excess delay time and

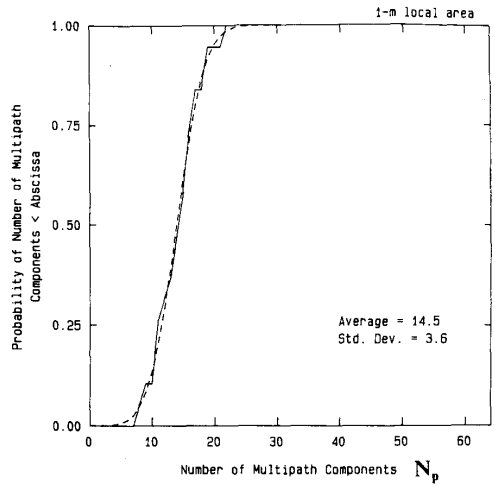

Fig. 6. An example of the distribution of the number of multipath components received in an individual profile for 19 profiles measured at discrete $\lambda/4$ receiver separations along a 1 m track. Gaussian: Average = 14.5, standard deviation = 3.6.

dividing by the total number of possible multipath components for each excess delay interval (475 possible components in LOS, 381 possible components in OBS). This assumes no correlation on the arrival times of multipath components (i.e., the multipath components in a given profile arrive independently but with different probabilities). This is different from models for urban mobile radio channels [13], [14] and office environments [2] where multipath components were modeled to arrive in clusters rather than independently. In the urban mobile radio environment, it was assumed in [13], [14] that multipath components arrived in clusters where $P_R(T_K)$ depends directly on whether or not a multipath component was received at T_{K-1}. In [2], multipath components were modeled to arrive in clusters with a mean cluster arrival rate Λ and a mean ray arrival rate (within a cluster) λ. However, open plan offices and factory buildings contain reflecting objects spread throughput the workspace (as opposed to clusters of buildings in the urban mobile radio environment or partitions in many office buildings), and yield power delay profiles [1] that have multipath power at random excess delays over a 500 ns period. In [20], [21] it was shown that with an insensitive receiver (high threshold) the number of paths roughly fits a Poisson distribution, which in turn implies a constant mean arrival rate of the number of multipath components over a given range of excess delays. However, as the receiver sensitivity is increased, the number of arriving components becomes less clustered than the Poisson distribution. In [21], it is shown that the data in [1] do not fit the arrival time models given in [2], [13], [14].

In line-of-sight topographies, $P_R(T_K, S_1)$ shown in Fig. 8(a) decreases from the maximum value near 1.0 at $T_K = 0$ ns (LOS pulse) to 0.1 at an excess delay of 500 ns. In obstructed topographies, $P_R(T_K, S_2)$ increases from 0.55 at an excess delay of 0 ns to a maximum of 0.7 at an excess delay of 75 ns, and then decreases exponentially as

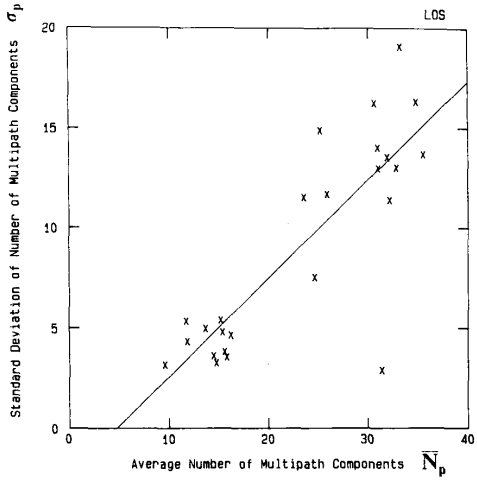

$$\sigma_p(S_1, P_n) = 0.492 \times (\overline{N}_p(S_1, P_n) - 4.77)$$

(a)

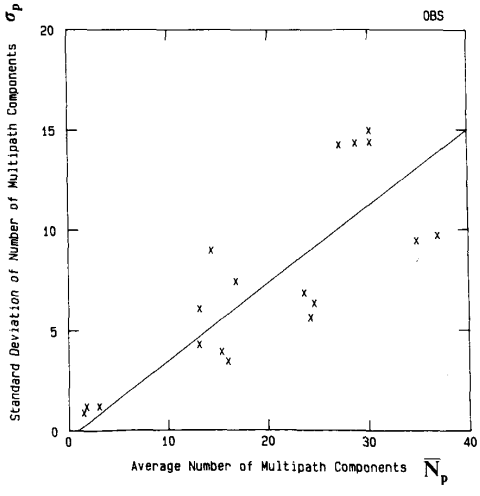

$$\sigma_p(S_2, P_n) = 0.383 \times (\overline{N}_p(S_2, P_n) - 0.89)$$

(b)

Fig. 7. Scatter plot of the Average and Standard Deviation of the number of multipath components received in an individual profile for 25 different 1 m local areas measured in a) LOS b) OBS topographies.

excess delay increases. This can be seen in Fig. 8(b) which shows the probability of multipath component arrival for OBS topographies at the lowest useful threshold. The probability is not 0 at an excess delay for 0 ns for OBS since synchronized time standards were not available, and the oscilloscope triggered on the first arriving energy. The probabilities for multipath arrivals may be modeled as piecewise functions of excess delay and are given as (8) and (9).

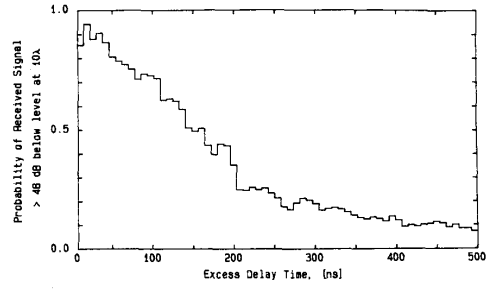

(a)

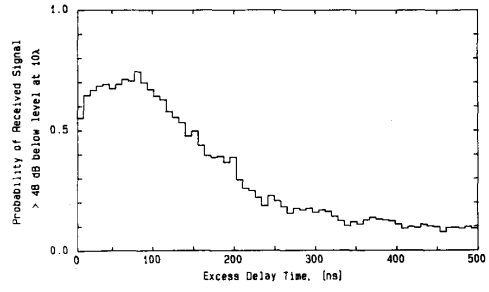

(b)

Fig. 8. Probability of receiving a multipath component within discrete excess delay intervals 7.8 ns wide for excess delays from 0 to 500 ns (a) LOS (b) OBS.

$$P_R(T_K, S_1) = \begin{cases} 1 - \dfrac{T_K}{367} & T_K < 110 \text{ ns} \\ 0.65 - \dfrac{(T_K - 110)}{360} & 110 \text{ ns} < T_K < 200 \text{ ns} \\ 0.22 - \dfrac{(T_K - 200)}{1360} & 200 \text{ ns} < T_K < 500 \text{ ns} \end{cases} \quad (8)$$

$$P_R(T_K, S_2) = \begin{cases} 0.55 + \dfrac{T_K}{667} & T_K < 100 \text{ ns} \\ 0.08 + 0.62e^{-\frac{(T_K - 100)}{75}} & 100 \text{ ns} < T_K < 500 \text{ ns} \end{cases} \quad (9)$$

where T_K takes on values which are integer multiples of 7.8 ns. In order to simulate profiles over small scale distances, (8) and (9) can be used with the path number distribution models in Section II-C and a recursive algorithm that repeatedly compares (8) or (9) with a uniformly distributed random variable until the proper N_p is generated for each profile. The algorithm, which is described in [20, pp. 99–101], [25], provides excellent agreement with observed small-scale multipath time-of-arrival data.

E. Large Scale Fading of Individual Multipath Components

The total power contained in a received multipath delay profile at a particular transmitter–receiver (T–R) separation of d meters is well described by the log-normal distribution (normal distribution with values in dB) about a mean path loss law in dB of the form $10 \times n \times \log(d)$ [1], [2], [6], and [22]. Values

of bn, the mean power path loss exponent, range from 1.8 to 2.8 for factory and open plan buildings where free-space path loss ($n = 2$) is assumed for the first 2.3 m (10λ). In multifloored partitioned office building, n's can range from 3 to 5 [26]. In this section we present models for the distribution of mean amplitudes of individual multipath components over the set P.

In general, the amplitude of an individual multipath component A_K depends on T_K, X_l, S_m, D_n, and P_n. We first remove' the (small scale fading) dependence on X_l for each excess delay interval T_K at each measurement location P_n by averaging over the 19 profiles to derive the mean (voltage) amplitudes $\overline{A}_K(T_K, S_m, D_n)$. Fig. 9 shows a scatter plot of the local means $\overline{A}_K(T_0, S_1, D_n)$ [in terms of relative attenuation in dB with respect to the amplitude received over a free space path at 2.3 m] versus the log distance within five buildings. Each data point represents the average amplitude of the first arriving multipath component for a given P_n measured in [1]. The best fit to the mean signal amplitude $\overline{A}_K$ is modeled by

$$\overline{A}_K(T_K, S_m, D_n)(\text{dB below } 10\lambda \text{ reference}) = 10 \times n(T_K, S_m) \times \log\left(\frac{D_n}{2.3}\right) \quad (10)$$

where $n(T_K, S_m)$ is the mean *power* path loss exponent that is both a function of excess delay and topography (but not distance), and D_n is in meters. Based on scatter plots similar to Fig. 9, which are given in [23], values of $n(T_K, S_m)$ were found by minimizing the mean square error between (10) and all $\overline{A}_K(T_K, S_m, D_n)$ values. Data from [1], [2], [7] suggest that in general, $n(T_K, S_m)$ increases with T_K (i.e., path loss is greater for components that arrive later in the profile). Fig. 10 shows the power law exponent $n(T_K, S_m)$ as a function of excess delay T_K for both LOS and OBS topographies. One might expect $n(T_0, S_1)$ to equal 2 (free space path loss) for LOS topographies. However, empirical data indicate that on the average the LOS signal attenuates more rapidly with distance than in free space. This is likely due to destructive interference caused by unresolved components (i.e., components caused by floor and ceiling reflections) which arrive within the first 7.8 ns of the measured profiles and smearing between adjacent bins imposed by data processing. In OBS topographies, the power of multipath components with small excess delay obeys a power law in which signals attenuate faster than in LOS ($n(T_K, S_2) > n(T_K, S_1)$). This is expected since shadowing due to obstructions causes attenuation to be greater than in unobstructed topographies [5]. The best fit values of $n(T_K, S_m)$ shown in Fig. 10 may be mathematically modeled as

$$n(T_K, S_1) = \begin{cases} 2.5 + \dfrac{T_K}{39} & T_K \le 15 \text{ ns} \\ 3.0 + \dfrac{T_K - 15.6}{380} & 15 \text{ ns} \le T_K \le 250 \text{ ns} \\ 3.6 & 250 \text{ ns} \le T_K \le 500 \text{ ns} \end{cases} \quad (11)$$

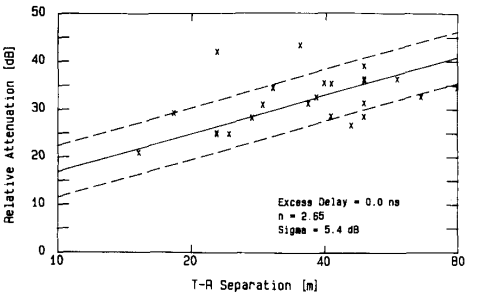

Fig. 9. Scatter Plot of large scale path attenuation versus $T-R$ separation for $T_K = 0$ in LOS topography. Attenuation is referenced to the signal received over an ideal free-space channel with $T-R$ separation of 10λ.

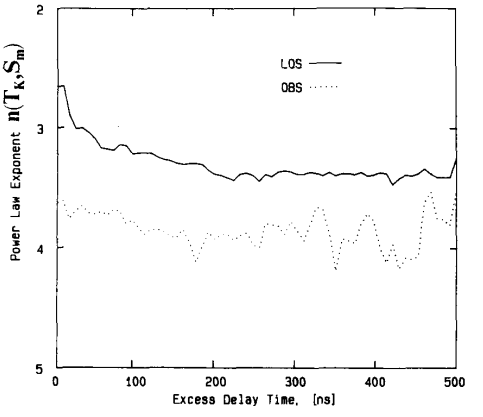

Fig. 10. Variation of power path loss exponent $n(T_K, S_m)$ with excess delay for LOS and OBS topographies.

$$n(T_K, S_2) = \begin{cases} 3.65 + \dfrac{T_K}{536} & T_K \le 310 \text{ ns} \\ 4.23 & 310 \text{ ns} \le T_K \le 500 \text{ ns} \end{cases} \quad (12)$$

where T_K takes on values which are integer multiples of 7.8 ns. Note that $n(T_K, S_2)$ does not fall off rapidly with increasing T_K. In [1], it was shown that sometimes multipath components in OBS topographies are strongest when they arrive 70 to 120 ns after the first detected signal.

Fig. 11 shows the cumulative distribution of all measured $\overline{A}_K(T_0, S_1, D_n)$, the first arriving (LOS) component, about (10) using the model in (11) for $n(T_0, S_1)$. Fig. 11 also shows the log-normal distribution about (10) with a standard deviation, denoted by $\sigma_{\text{large-scale}}$ of 5.4 dB. This illustrates that not only is the *total* received power log-normally distributed about the mean [1], [5], [22], but the mean *individual* multipath component powers are also log-normally distributed about the mean power law given in (10) over large scale distances. The standard deviation $\sigma_{\text{large-scale}}(S_m)$ of the local mean amplitudes $\overline{A}_K(T_K, S_m, D_n)$ about the mean path loss model in (10)–(12) has been found to be relatively insensitive to excess delay and is modeled as 4 dB for LOS and 5 dB for OBS topographies [20], [23]. The large scale standard deviation of multipath component amplitudes for obstructed

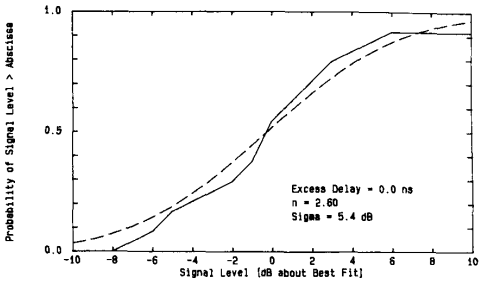

Fig. 11. Distribution of large scale path attenuation about $10 \times n(T_K, S_m) \times \log(D_n)$ model. The dotted line represents the log-normal distribution about the mean value with a standard deviation of 5.4 dB.

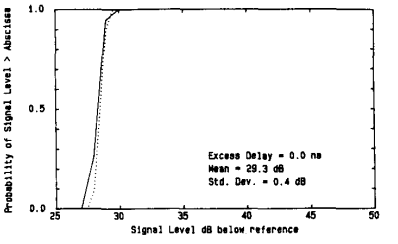

Fig. 12. Distribution of 19 individual multipath component amplitudes over a 1 m local area at a constant excess delay of $T_K = 0$ ns. The dotted line represents the log-normal distribution with a mean = 29.3 dB below a 10λ free space path hoss reference and a standard deviation = 0.4 dB.

topographies is slightly larger because the effects of shadowing cause greater variation in path attenuation as the receiver is moved from one local area to another. Extensive data reduction and curve fitting to develop these models can be found in [20] and [23].

F. Small Scale Signal Fading on Individual Multipath Components

The models in section E are useful for predicting mean values of multipath amplitudes at particular excess delays over a wide range of $T-R$ separations. However, multipath amplitudes fade as a receiver is moved along a local area. We now present the statistics of the fading of individual components which occur as a result of small changes in receiver location. Such models can provide insight into jitter, equalizer requirements, and when combined with assumptions or knowledge of phase information, enables a wide-band channel model to recreate realistic narrow-band fading statistics [1, eq. (14)].

We have shown in [20], [23] that the small scale fading is well described by a log-normal distribution about the local mean where the standard deviation is a random variable. Fig. 12 shows an example of the cumulative distribution function of the 19 multipath signal amplitudes $A_K(T_0, X, S_1, D_6, P_6)$ in Fig. 2. The dotted line in Fig. 12 is the log-normal (normal in dB) distribution with a local mean $\overline{A}_K(T_0, S_1, D_6, P_6) = 29.3$ dB below a 10λ reference and standard deviation $\sigma_{\text{small-scale}}(T_0, S_1, P_6) = 0.4$ dB about the mean. $\sigma_{\text{small-scale}}(T_K, S_m, P_n)$ describes the variation of the individual A_K's about the mean within a local area and is modeled as a random variable for each P_n. The distribution of $\sigma_{\text{small-scale}}(T_K, S_m, P_n)$ based on empirical data is given in (13) and Fig. 13. The small value for $\sigma_{\text{small-scale}}$ in Fig. 12 indicates the particular multipath component is virtually specular. Numerous plots similar to Fig. 12 are given in [20], [23] and confirm that the log-normal distribution describes the small scale finding at various locations and excess delays. The fact that local fading of individual components is log-normal and not Rayleigh is similar to models in [13] for urban mobile radio channels. Because of the excellent temporal resolution of the models, the shallow log-normal fading is due to specular-like scattering mechanisms which behave similarly over the transmission bandwidth and local area.

We have found that over the ensemble of measurements, the

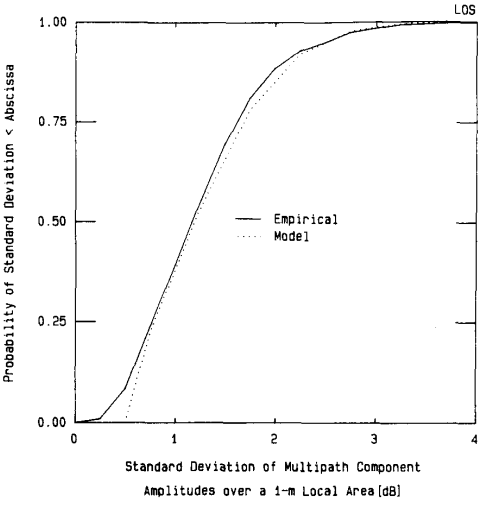

Fig. 13. cdf of measured standard deviation (in dB) $\sigma_{\text{small-scale}}(T_K, S_m)$ of multipath component amplitudes over a local area.

degree of small scale log-normal fading about the local mean is not dependent upon excess delay [20]. Thus, where multipath components at $T_K = 0$ undergo very slight fading over certain measurement locations such as in Figs. 2 and 12, at other locations the first arriving component fades as much as signals arriving later in the profile due to several signals arriving within the path resolution of the measurement system and shadowing. Similarly, at some locations, signals which arrive later in the profile do not fade (they are specular reflections from walls, etc.), whereas at other locations, signals with large excess delay fade significantly due to shadowing or multiple signals arriving within the resolution of the measurement apparatus. The cumulative distribution function F for $\sigma_{\text{small-scale}}(T_K, S_m, P_n)$ about $\overline{A}_K(T_K, S_m, D_n, P_n)$ over 1-m local areas for any excess delay interval has been found to closely fit [20]

$$F(\sigma_{\text{small-scale}}(T_K, S_m, P_n)) = 1 - \exp\left(\frac{-(\sigma_{\text{small-scale}}(T_K, S_m, P_n) - a)^2}{2}\right) \quad (13)$$

where the offset parameter $a = 0.25$ dB for LOS and 0.50 dB for OBS topography locations and the value of $\sigma_{\text{small-scale}}(T_K, S_m, P_n)$ in (13) is in dB. The empirical cumulative distribution for $\sigma_{\text{small-scale}}(T_K, S_1)$ and the model (13), are shown in Fig. 13. Although the distribution of $\sigma_{\text{small-scale}}$ is the same for all excess delays, the actual value of $\sigma_{\text{small-scale}}(T_K, S_m, P_n)$ is random and independent for each excess delay T_K at each P_n. Thus, from (10)–(13), the amplitude of an individual multipath component obeys log-normal statistics of the form:

$$A_K(T_K, X_l, S_m, D_n, P_n) = N\left[N\left[10 \times n(T_K, S_m) \times \log\left(\frac{D_n}{2.3}\right),\ \sigma^2_{\text{large-scale}}(S_m)\right],\ \sigma^2_{\text{small-scale}}(T_K, S_m, P_n)\right] \quad (14)$$

where $N[\overline{x}, \sigma_x^2]$ represents the normal distribution with mean $\overline{x}$ (in dB) and standard deviation σ_x (in dB). Equation (14) incorporates both large scale and small scale fading on individual multipath component amplitudes, and can be implemented easily in simulation.

G. Correlation Coefficient Function

The relative distances and excess delay values at which individual multipath signal amplitudes $A_K(T_K, X_l, S_m, D_n)$ become uncorrelated are important for the analysis of antenna diversity and equalization. Inspection of the empirical data led us to believe that within a local area, some of the multipath amplitudes at various locations and excess time delays are correlated. We assume that over distance separations greater than several wavelengths, channels become uncorrelated in space. That is, the amplitude of a multipath component at a particular excess delay will be uncorrelated with the amplitude of a component measured by a distant receiver at the same excess delay. Over excess delay differences greater than a few hundred nanoseconds, we assume multipath signal strengths become uncorrelated since the reflections are due to different physical structures within the building.

In Section II-F, we showed the amplitudes of individual components are well modeled by a log-normal fading distribution as a mobile is moved along a 1 m track. We assume that two multipath component amplitudes $A_K(T_K, X_l, S_m, D_n)$ and $A_K(T_K, X_l + \Delta X, S_m, D_n)$, or $A_K(T_K, X_l, S_m, D_n)$ and $A_K(T_K + \Delta T, X_l, S_m, D_n)$, are also *jointly* log-normally distributed over 1 m local areas. Although this is not necessarily true, it provides a tractable method in which to compute correlation coefficients for use in a channel simulator [14].

In general, the conditional distribution of $A(\xi_2)$ given the value of $A(\xi_1)$ can be calculated by assuming both random variables form a jointly log-normal distribution with a conditional mean

$$\overline{A(\xi_2)}|A(\xi_1) = \overline{A(\xi_2)} + \rho(\xi_1, \xi_2)\left(A(\xi_1) - \overline{A(\xi_1)}\right)\frac{\sigma_{A(\xi_2)}}{\sigma_{A(\xi_1)}} \quad (15a)$$

and a conditional variance

$$\sigma^2_{A(\xi_2)|A(\xi_1)} = \left(1 - \rho^2(\xi_1, \xi_2)\right)\sigma^2_{A(\xi_2)} \quad (15b)$$

where A is a multipath amplitude. The variable ξ represents both the spatial location X_l and excess delay T_K. $\rho(\xi_1, \xi_2)$ is the spatial or temporal correlation function of multipath amplitudes. In (15), means and standard deviations have values in dB. For spatial correlation, the variables in (15) represent [24]

$$A(\xi_1) = A_K(T_K, X_l, S_m, D_n)$$
$$A(\xi_2) = A_K(T_K, X_l + \Delta X, S_m, D_n)$$
$$\sigma_{A(\xi_1)} = \sigma_{A(\xi_2)} = \sigma_{\text{small-scale}}(T_K, S_m, P_n)$$

where ΔX is the spatial separation between profiles and takes on integer values of $\lambda/4$. For temporal correlation, the variables represent [24]

$$A(\xi_1) = A_K(T_K, X_l, S_m, D_n)$$
$$A(\xi_2) = A_K(T_K + \Delta T, X_l, S_m, D_n)$$
$$\sigma_{A(\xi_1)} = \sigma_{\text{small-scale}}(T_K, S_m, P_n)$$
$$\sigma_{A(\xi_2)} = \sigma_{\text{small-scale}}(T_K + \Delta T, S_m, P_n)$$

where ΔT is the excess delay difference between two arriving multipath components in the same profile, and is a multiple of 7.8 ns.

1) Spatial Correlation: Spatial correlation is a measure of the correlation between the amplitudes of multipath components which arrive with the same excess delay in different profiles X_l in a particular measurement location P_n. The spatial correlation coefficient function of the measured data averaged over different measurement areas for LOS and OBS topographies varies with space and excess delay. Spatial correlation coefficient functions in each local area P_n were computed in [20], [23] by (16) where $E[\,]$ is the expected value at a particular P_n. In (16), the dependence of S and D is implicit for a specific P_n, and $\rho(T_K, \Delta X)$ was computed in [23] for all possible values of T_K where at least 5 of the 19 multipath components exist over the local area. ΔX ranged between 0 and 4λ. The model for the average spatial correlation coefficient function for LOS topographies was computed as the average of the correlation coefficient functions

$$\rho(T_K, \Delta X) = \frac{E\left[\left(A_K(T_K, X_l) - \overline{A_K(T_K, X_l)}\right)\left(A_K(T_K, X_l + \Delta X) - \overline{A_K(T_K, X_l + \Delta X)}\right)\right]}{\sqrt{E\left[\left(A_K(T_K, X_l) - \overline{A_K(T_K, X_l)}\right)^2\right]E\left[\left(A_K(T_K, X_l + \Delta X) - \overline{A_K(T_K, X_l + \Delta X)}\right)^2\right]}} \quad (16)$$

computed at each measurement location [23], and is shown in Fig. 14. As seen in Fig. 14, multipath component amplitudes become uncorrelated at spatial separations of $\lambda/2$ and become slightly anticorrelated for separations of 2.5 to 3λ at excess delays less than 100 ns. At all excess delays greater than 100 ns, multipath components are uncorrelated for separations greater than $\lambda/2$. The equation for the spatial correlation coefficient function for the LOS multipath component, denoted by $\rho(T_0, \Delta X, S_1)$, is

$$\rho(T_0, \Delta X, S_1) = 1 - \frac{3.2\Delta X}{\lambda} \quad \left(\text{for } \Delta X < \frac{\lambda}{4}\right)$$
$$= 0.41e^{-\left(\frac{\Delta X - \lambda/4}{\lambda/1.9}\right)} - 0.21 + 0.21 \cdot \left[1 - e^{-\left(\frac{\Delta X - 2.5\lambda}{\lambda/3.6}\right)}\right] u(\Delta X - 2.5\lambda)$$
$$\left(\text{for } \frac{\lambda}{4} \leq \Delta X < 4\lambda\right) \tag{17}$$

where ΔX is the separation between profiles in meters, $u(\ )$ is the unit step function, and $\lambda = 0.23$ m at 1300 MHz. In order to model the spatial correlation coefficient of later arriving multipath components, a decaying exponential model was used and a minimum mean squared error fit was used to determine the exponential function. The spatial LOS correlation coefficient function for all path amplitudes arriving after the LOS path was found in [23] to be

$$\rho(T_K, \Delta X, S_1) = \rho(T_0, \Delta X, S_1) \times e^{-\frac{T_K}{170}} \tag{18}$$

with T_K in nanoseconds. In [25], an extension of (15) is used to implement the LOS spatial correlation function in the SIRCIM software simulator.

In obstructed topographies, the average spatial correlation was found to be very close to $\rho(T_K, \Delta X, S_2) = \delta(T_K, 0, S_2)$. That is, the A_K's are uncorrelated for all receiver separations and excess delays. Nonzero correlation coefficients exist for a particular P_n, but on the average, multipath component amplitudes are uncorrelated in obstructed topography locations.

2) Temporal Correlation: Temporal correlation is the measure of the correlation of the amplitudes about the local mean amplitude of multipath components which arrive with different excess delays within the same profile X_l. Temporal correlation coefficient functions for each local area P_n were computed using (19), [20].

The model of the average temporal correlation coefficient function for LOS topographies is shown in Fig. 15, and was computed as the average of the correlation coefficient functions (19) computed at each measurement location P_n. $\rho(T_K, \Delta T)$ was computed in [23] for all values of T_K where at least 5 of the multipath components existed at both T_K and $T_K + \Delta T$

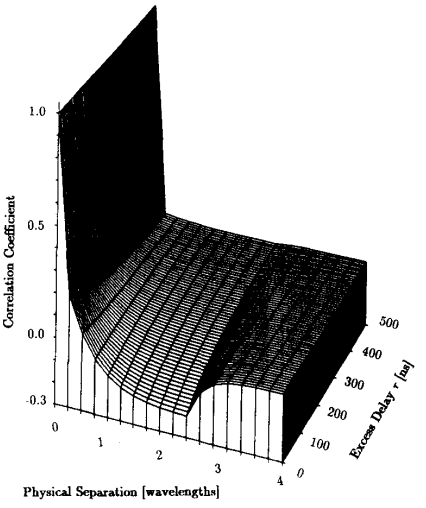

Fig. 14. Average spatial correlation coefficient function model for LOS topographies.

over each local area. In the case of LOS topography, with the first signal arriving at $T_K = 0$ ns, the amplitude of a signal arriving with an excess delay of $\Delta T = 7.8$ ns can be seen in Fig. 15 to be nearly uncorrelated. A signal arriving at an excess delay of $\Delta T = 15.6$ ns will be anticorrelated with the amplitude of the signal at $T_K = 0$ ns. Amplitudes of signals which arrive at 16 ns $< T_K + \Delta T < 50$ ns will be slightly anticorrelated with the amplitude at $T_K = 0$ ns. For $T_K > 0$ ns, multipath component amplitudes become uncorrelated at $T_K + \Delta T = 25$ ns and do not become anticorrelated for any time delay separation.

In obstructed topography, multipath component amplitudes become uncorrelated for excess delay separations of 25 ns [20], regardless of T_K. The equations of the models of the temporal correlation coefficient function were found in [20], [23] to be

$$\rho(T_0, \Delta T, S_1) = \begin{cases} A \exp\left(-\frac{\Delta T}{C}\right) - B & \text{for } T_K = 0 \text{ ns and } \Delta T \leq 15.6 \text{ ns} \\ D \exp\left(-\frac{(\Delta T - 15.6)}{E}\right) & \Delta T > 15.6 \text{ ns} \end{cases}$$

$$\rho(T_K, \Delta T, S_1) = \exp\left(-\frac{\Delta T}{F}\right) \qquad T_K > 0 \tag{20}$$

and

$$\rho(T_K, \Delta T, S_2) = \exp\left(-\frac{\Delta T}{G}\right) \qquad T_K \geq 0 \tag{21}$$

$$\rho(T_K, \Delta T) = \frac{E\left[\left(A_K(T_K) - \overline{A_K(T_K)}\right)\left(A_K(T_K + \Delta T) - \overline{A_K(T_K + \Delta T)}\right)\right]}{\sqrt{E\left[\left(A_K(T_K) - \overline{A_K(T_K)}\right)^2\right] E\left[\left(A_K(T_K + \Delta T) - \overline{A_K(T_K + \Delta T)}\right)^2\right]}}. \tag{19}$$

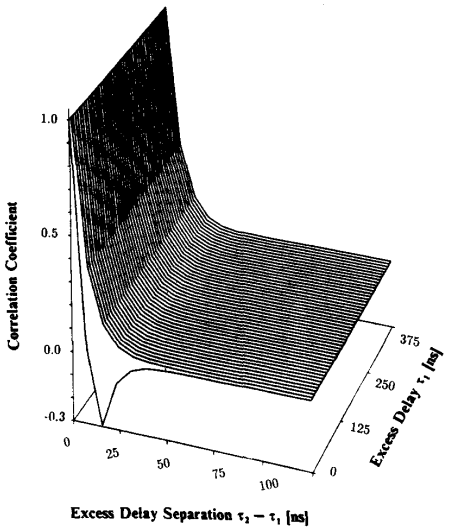

Fig. 15. Average temporal correlation coefficient function model for LOS topographies.

where

$$\begin{aligned} A &= 1.440 \\ B &= 0.440 \\ C &= 6.821 \\ D &= -0.301 \\ E &= 7.029 \\ F &= 7.665 \\ G &= 6.493 \end{aligned} \tag{22}$$

and T_K is in nanoseconds.

III. Simulation Results

An important consideration in the evaluation of statistical models is their likeness to physical measurements. Simulated profiles must possess similar time dispersion and path loss statistics over an ensemble of simulated measurements and must *look* like actual measured data. Figs. 16 and 17 give examples of channel impulse responses for simulated LOS and OBS topographies over a 1 m local area. Simulation was accomplished by choosing random values of $T-R$ separation (D_n) for a particular topography (S_m) and then using random number generators in a computer program to drive the statistical models given in (6)–(22). From comparison with Figs. 2 and 3, it can be seen that the simulated profiles represent viable multipath channel impulse responses for open plan building radio channels and are very similar to those reported in [1] and [9]. The number of multipath components N_p changes from profile to profile and multipath amplitudes fade as the simulated receiver is moved along a 1 m track. The distribution of the number of multipath components, the probability of receiving multipath components at particular excess delays, and the amplitude of multipath components over large scale and small scale areas are very accurately recreated [20].

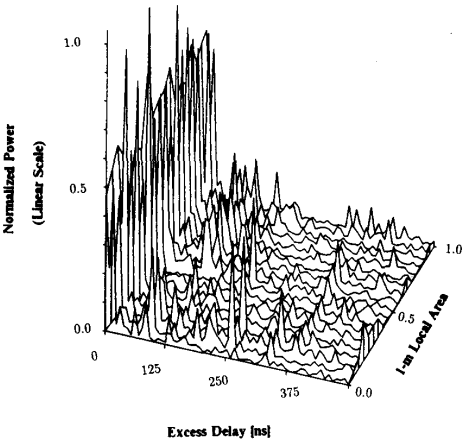

Fig. 16. Example of simulated LOS profiles for 19 discrete locations along a 1 m track.

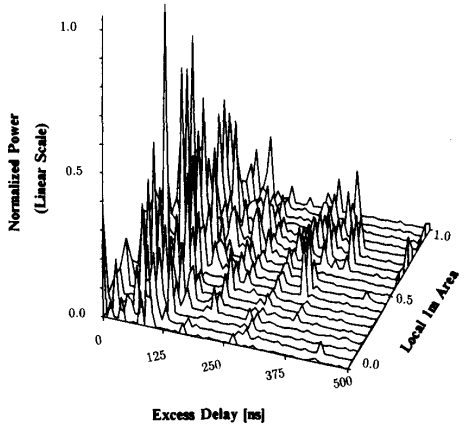

Fig. 17. Example of simulated OBS profiles for 19 discrete locations along a 1 m track.

Rms delay spread is a common measure of the temporal dispersion of a multipath channel impulse response. A set of 19 equally spaced local area profiles was generated for each of 25 LOS and 25 OBS locations using random values of D_n for each location. A computer program implemented (6)–(21) to provide the 50 simulated measured locations (950 profiles) in a Monte–Carlo fashion. This simulation provided a computer-generated data base of the same size as measured in [1]. The cdf's of the rms delay spread for the simulated radio channels using the models presented here are shown on Fig. 4 for both LOS and OBS topographies. The median values of rms delay spread are approximately 80 ns for LOS and 95 ns for OBS topographies. These are slightly smaller than the values (95 ns for LOS and 105 ns for OBS) of the empirical data collected in [1]. The models used in the simulation, however, were determined based on a subset of the data in [1] which did not include two of the most time-dispersive measurement locations.

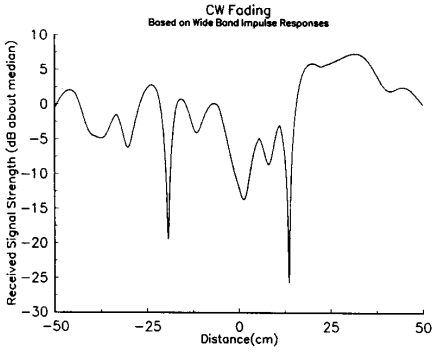

Fig. 18. Example of simulated CW envelope fading along a 1 m track in LOS topography based on wide-band impulse response models presented in this paper. A simple technique is used to synthesize the spatially varying phase of each individual multipath component. Velocity assumed to be 0.25 m/s.

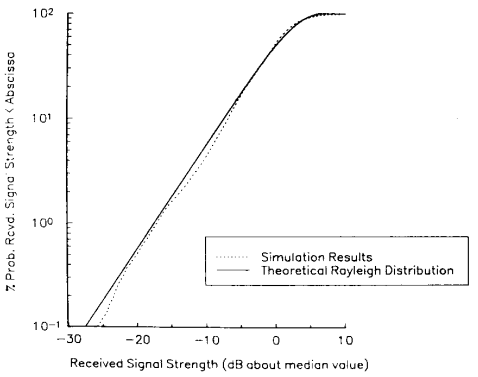

Fig. 19. cdf of simulated CW envelope fading (about the local medians) at 25 LOS and 25 OBS locations. Also shown is theoretical Rayleigh distribution. The simulated results are extremely close to those measured in [5, Fig. 7].

To further test the accuracy of the statistical models, we investigated the ability of the simulator to recreate narrow-band (CW) fading based upon the wide-band models. For a given local area, approximately 50 equally spaced wide-band profiles were generated between each of the original 19 wide-band profiles by performing cubic spline interpolation of the A_K's. Since no phase information is available in (3), phases of individual multipath components in each profile were synthesized in a manner described in [20] and [25]. Random phases and scattering geometries were generated for the multipath components in the first power profile in a local area, and all subsequent profiles within a local area used phases that were deterministically derived from simple geometry under the assumption that the scatterers remained fixed in position as the receiver moved along a 1 m track. The magnitude of the phasor sum of all multipath components in a profile was then computed to give a CW envelope voltage for a particular location along the track [25]. Note that the statistical models ignore the temporal fading effects, since it has been shown in [1], [5] that the temporal fading of individual multipath components is very slight, which leads to tame Rician fading channels ($K = 10$ dB) for stationary terminals. Doppler shifts, however, are computed for each multipath component and slightly affect the spatially varying phase of each component. Fig. 18 shows how this simulation approach yields a typical simulated CW fading signal as a receiver is moved along a 1 m track. First and second-order statistics of small-scale and large-scale fading and path loss are nearly identical to CW measurements reported in [5]. Fig. 19 shows the cdf of small-scale received envelope voltages about the local median value for 25 simulated LOS and 25 OBS measurement locations. Notice that the cdf is close to Rayleigh, and appears log-normal below the median. This is identical to measured results in [5, Fig. 7]. The level crossing rates of the CW envelope for the 50 simulated locations is shown in Fig. 20. Also shown in the figure is the level crossing rates for the theoretical Rayleigh distribution. Comparison of Figs. 18–20 with actual field measurement data indicate that the statistical impulse response models provide very realistic narrow-band channels when a simple phase synthesis technique is used.

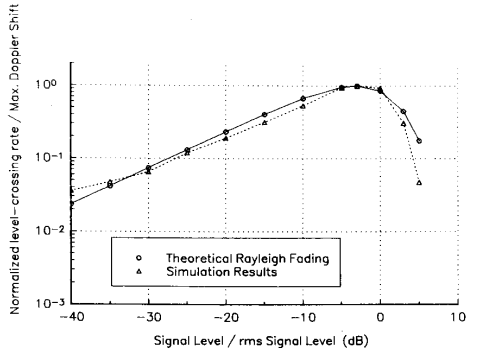

Fig. 20. Level crossing rates of simulated CW fading signals along 1 m tracks at 50 locations. Also shown are theoretical level crossing rates for Rayleigh-fading signals. Velocity assumed to be 0.25 m/s.

Fig. 21 shows simulated wide-band path loss values for 25 LOS and 25 OBS measurement locations in open plan buildings where each simulated location corresponds to a 1 m local area. Fig. 21 compares extemely well to scatter plots in [1].

It should be noted that wide-band and narrow-band path loss and fading statistics generated with the above models provide excellent agreement with empirical data [1], [5]. Complete simulation results are contained in [20], and a simulation program and source code SIRCIM is available from Virginia Tech. The models presented here will be refined as more data from different environments and frequency bands become available.

IV. Conclusion

We have presented statistical models for wide-band power impulse responses inside open plan buildings. These models

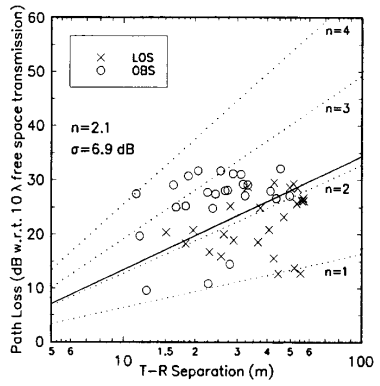

Fig. 21. Example of 50 simulated wide-band path loss values using wide-band models given in this paper. The scatter plot is representative of those produced by the SIRCIM simulator.

are based on propagation measurements from five factory buildings and statistically characterize the impulse responses of open plan building radio channels at 1300 MHz. Measurements in [9] show these models also hold at 4.0 GHz.N_p, the number of multipath components which arrive at a receiver over a 1 m local area, has been shown to be Gaussian distributed (Fig. 6) about a mean $\overline{N}_p$ that ranges between 9 and 36. The standard deviation of N_p (over a particular 1 m local area) is linearly related to the $\overline{N}_p$ for that local area [Fig. 7 and (6) and (7)]. The likelihood of receiving multipath components at a particular excess delay have been shown to have a maximum near $T_K = 0$ ns for LOS and $T_K = 75$ ns for OBS topographies, and decreases as excess delay increases [Fig. 8 and (8) and (9)]. The mean amplitude of multipath components within 1 m local areas has been shown to be log-normally distributed about an average large scale power path loss model of the form $10 \times n(T_K, S_m) \times \log(D_n)$ [Figs. 10 and 11 (10)–(12), (14)]. The distribution of individual multipath component amplitudes within a local area has been shown to be log-normally distributed about the local mean (Fig. 12). Multipath component amplitudes have been found to be correlated for distance separations less than 3λ and temporal separations less than 100 ns [Figs. 14 and 15 and (18), (20), and (21)].

It should be noted that all models are *simple* models in that they can be (and have been) programmed in a personal computer. The most salient feature, however, is that the models reproduce multipath channel conditions that are very realistic since they are based on real world measurements, and may thus be used for meaningful system analyses in factories and open plan buildings. In addition, simulation of other multipath channels is possible based on the framework of the models presented in this paper by changing the values of the models presently used. Thus, it will not be difficult to incorporate wide-band models of multipath channel behavior measured in different mobile and portable radio environments and at different frequencies as empirical data become available.

ACKNOWLEDGMENT

The authors thank V. Fung for using SIRCIM to produce Figs. 8–21.

REFERENCES

[1] T. S. Rappaport, "Characterization of UHF multipath radio propagation inside factory buildings," *IEEE Trans. Antennas Propagat.*, vol. 37, pp. 1058–1069, Aug. 1989.
[2] A. A. M. Saleh, and R. A. Valenzuela, "A statistical model for indoor multipath propagation," *IEEE J. Select Areas Commun.*, vol. SAC-5, pp. 128–137, Feb. 1987.
[3] R. A. Valenzuela, "Performance of adaptive equalization for indoor radio communications," *IEEE Trans. Commun.*, vol. 37, pp. 291–293, Mar. 1989.
[4] J. C.-I. Chuang, "The effects of time delay spread on portable radio communications channels with digital modulation," *IEEE J. Select Areas Commun.*, vol. SAC-5, pp. 879–889, June 1987.
[5] T. S. Rappaport and C. D. McGillem, "UHF fading in factories," *IEEE J. Select Areas Commun.*, vol. 7, pp. 40–48, Jan. 1989.
[6] ——, "Indoor radio communications for factories of the future," *IEEE Commun. Mag.*, vol. 27, pp. 15–24, May 1989.
[7] D. M. J. Devasirvatham, "Multipath time delay spread in the digital portable radio environment," *IEEE Commun. Mag.*, vol. 25, pp. 13–21, June 1987.
[8] R. J. C. Bultitude, S. A. Mahmoud, and W. A. Sullivan, "A comparison of indoor radio propagation characteristics at 910 MHz and 1.75 GHz," *IEEE J. Select Areas Commun.*, vol. 7, pp. 20–30, Jan. 1989.
[9] D. A. Hawbaker and T. S. Rappaport, "Indoor wideband radiowave propagation measurements at 1.3 GHz and 4.0 GHz," *Electron. Lett.*, vol. 26, no. 21, pp. 1800–1802, Oct. 11, 1990.
[10] P. Yegani and C. D. McGillem, "A statistical model for line-of-sight (LOS) factory radio channels," in *39th Vehic. Technol. Conf. Proc.*, San Francisco, CA, May 1989, pp. 496–500.
[11] G. L. Turin, "Communication through noisy, random-multipath channels," in *IRE Nat. Conf. Rec.*, pp. 4, 1956, pp. 154–166.
[12] G. L. Turin, F. D. Clapp, T. L. Johnson, S. B. Fine, and D. Lavry, "A statistical model for urban multipath propagation," *IEEE Trans. Vehic. Technol.*, vol. VT-21, pp. 1–9, Feb. 1972.
[13] H. Suzuki, "A statistical model for urban radio propagation," *IEEE Trans. Commun.*, vol. COM-25, pp. 673–680, July 1977.
[14] H. Hashemi, "Simulation of urban radio propagation," *IEEE Trans. Vehic Technol.*, vol. VT-28, pp. 213–225, Aug. 1979.
[15] W. C. Y. Lee, *Mobile Communications Engineering.* New York: McGraw-Hill, 1982.
[16] J. P. de Weck, P. Merki, and R. Lorenz, "Power delay profiles measured in mountainous terrain," in *38th IEEE Vehic. Technol. Conf. Proc.*, Philadelphia, PA, June 1988, pp. 105–112.
[17] D. C. Cox and R. P. Leck, "Distribution of multipath delay spread and average excess delay for 910 MHz urban mobile radio paths," *IEEE Trans. Antennas Propagat.*, vol. AP-23, pp. 206–213, Mar. 1975.
[18] T. S. Rappaport, S. Y. Seidel, and R. Singh, "900 MHz multipath propagation measurements for U.S. digital cellular radiotelephone," *IEEE Trans. Vehic. Technol.*, vol. 39, pp. 132–139, May 1990.
[19] J. G. Proakis, *Digital Communications.* New York: McGraw-Hill, 1989.
[20] S. Y. Seidel, "UHF indoor radio channel models for manufacturing environments," Masters thesis in electrical engineering, Virginia Polytech. Inst. State Univ., Blacksburg VA, Aug. 1989.
[21] T. S. Rappaport, "Radio channel modeling in manufacturing environments, Part 1," intermediate Rep. Res. Comput. Integrated Design, Manufacturing, and Automat. Cent. Purdue Univ., Dec. 15, 1988.
[22] D. C. Cox, H. Arnold, and P. Porter, "Universal digital portable communications—A system perspective," *IEEE Trans. J. Select Areas Commun.*, vol. SAC-5, pp. 764–773, June 1987.
[23] T. S. Rappaport, "Radio channel modeling in manufacturing environments, Parts 2 and 3," Intermediate Rep. Res. Comput. Integrated Design, Manufact., and Automat. Cent., Purdue Univ., Feb. 28, 1989.
[24] S. Y. Seidel, K. Takamizawa, and T. S. Rappaport, " Application of second-order statistics for an indoor radio channel model," in *39th IEEE Vehic. Technol. Conf. Proc.*, San Francisco, CA, May 1989, pp. 888–892.
[25] S. Y. Seidel and T. S. Rappaport, "Simulation of UHF indoor radio channels for open plan building environments," in *40th IEEE Vehic. Technol. Conf. Proc.*, Orlando, FL, May 1990, pp. 597–602.
[26] ——, "900 MHz path loss measurements and prediction techniques for in-building communication system design," in *Proc. 41st IEEE Vehic. Technol. Conf.*, St. Louis, MO, May 21, 1991, pp. 613–618.

Theodore S. Rappaport (S'83–M'87) was born in Brooklyn, NY, on November 26, 1960. He received the B.S.E.E., M.S.E.E., and Ph.D. degrees from Purdue University in 1982, 1984, and 1987, respectively.

In 1983 and 1986 he was employed with Harris Corporation, Melbourne, FL. From 1984 to 1988 he was with the NSF Engineering Research Center for Intelligent Manufacturing Systems at Purdue University. In 1988, he joined the Electrical Engineering faculty of Virginia Tech, where he is Assistant Professor and Director of the Mobile and Portable Radio Research Group. He conducts research in mobile radio communication system design and RF propagation prediction through modeling, and consults often in these areas.

Dr. Rappaport has authored or coauthored more than 30 technical publications in the areas of indoor radio propagation, vehicular navigation, ionospheric propagation, and wide-band communications, and holds a U.S. patent for a wide-band antenna. In 1990, he received the Marconi Young Scientist Award for his contributions in indoor radio communications. He is an active member of the IEEE Communications and Vehicular Technology Societies, Senior Editor for IEEE JOURNAL ON SELECTED AREAS IN COMMUNICATIONS, and is a member of ASEE, Eta Kappa Nu, Tau Beta Pi, Sigma Xi, Radio Club of America, and is a life member of the ARRL.

Scott Y. Seidel (S'89) was born in Falls Church, VA, in 1966. He received the B.S. and the M.S. degrees and in electrical engineering from Virginia Polytechnic Institute and State University, Blacksburg, in 1988 and 1989, respectively. He is currently pursuing the Ph.D. degree in electrical engineering at Virginia Polytechnic Institute and State University under the support of an NSF Graduate Research Fellowship.

He has had industrial experience as a co-op working summers at Bendix Field Engineering, Columbia, MD, throughout his undergraduate career. He has been involved in the development of both indoor and urban microcellular radio channel models and is interested in propagation prediction and system design.

Mr. Seidel is a member of Tau Beta Pi, Eta Kappa Nu, and Phi Kappa Phi.

Koichiro Takamizawa (S'87) was born in Fukuoka, Japan, in 1961. He received the B.S. degree from Rensselaer Polytechnic Institute, Troy, NY, in 1985, and the M.S. degree from Virginia Polytechnic Institute and State University, Blacksburg, VA, in 1988, both in electrical engineering. He is currently pursuing the Ph.D. degree also in electrical engineering.

Since 1987 he has been working at the Satellite Communications Group, Virginia Polytechnic Institute and State University as a Graduate Research Associate. His research interests include electromagnetic theory, antennas, and satellite, and portable radio communications.